Integrated local control of active power and voltage support for three-phase three-wire converters

Please check the document version of this publication:

• A submitted manuscript is the version of the article upon submission and before peer-review. There can be important differences between the submitted version and the official published version of record. People interested in the research are advised to contact the author for the final version of the publication, or visit the DOI to the publisher's website.
• The final author version and the galley proof are versions of the publication after peer review.
• The final published version features the final layout of the paper including the volume, issue and page numbers.

Link to publication

Integrated Local Control of Active Power and Voltage Support for Three-Phase Three-Wire Converters

Ya Zhang, Gabriel Tibola, Maurice G. L. Roes, Jorge L. Duarte
Department of Electrical Engineering
Eindhoven University of Technology
Eindhoven, The Netherlands
ya.zhang@tue.nl

Abstract—The derivation of a robust control algorithm is presented to provide decoupled active power regulation and local grid voltage support in three-phase three-wire grid-connected converters (GCCs). Unlike conventional control schemes, the proposed strategy is designed to be harmonic sequence asymmetric for the purpose of local voltage unbalance correction. A frequency-domain Norton equivalent model is derived to illustrate the working principle of the strategy. Accordingly, by following a frequency-domain decoupled method, the fundamental positive-sequence, the harmonic symmetrical sequences and the fundamental negative-sequence components are regulated independently. Consistent to the model analysis, simulation results validate reduction of local voltage unbalance and total harmonic distortion. Since no external sensors are required for the implementation of the strategy, it is a local approach, applicable to already-existing GCC systems. Moreover, in view of the higher switching frequencies as attainable by devices from the next SiC generation, the accuracy and dynamic behavior of the control algorithms can be much enhanced, improving therefore the quality of the processed energy.

Index Terms—Grid-interactive power converters, control, voltage unbalance, harmonics, compensation.

I. INTRODUCTION

Unbalanced voltages cause adverse effects on electrical loads and power distribution networks. Compensation for voltage unbalance is usually implemented using an active power filter acting as a voltage source in series with the power distribution line [1]. Another solution is to apply a shunt converter behaving as a current source to absorb or share the unbalanced currents [2], [3]. However, most local voltage support strategies are based on measuring the polluting load current, being therefore not always easy to implement, especially when multiple loads are present. Hence, the application of shunt converters to enhance the local voltage quality on the basis of local measurements, which are not taken beyond the converter's point of common coupling (PCC), has received increasing attention in recent years [4]–[10].

However, limited research has been carried out on how to correct the negative-sequence component and harmonics at the same time by means of three-phase grid-connected converters using only local measurements. Specifically, discussion on three-phase local voltage support is mostly carried out in the synchronous reference frame, making it difficult to build a natural analogy between single-phase and three-phase converters when talking about harmonic compensation, particularly in the context of Norton equivalent model derivation.

In this paper an integrated control method that decouples active power regulation and local voltage support for a three-phase three-wire GCC system is proposed on the basis of only stationary reference frames. The active power regulation is achieved by accurate control of the GCC output current fundamental positive-sequence component. Simultaneously, local voltage support is realized by providing an adjustable low-impedance path (through the GCC) for the unbalanced and harmonic components coming from the grid network. By doing so, the distorting current components, as introduced by local asymmetrical or non-linear loads, take the path through the GCC, instead of flowing towards the grid.

In Section II the GCC system architecture and control strategy are briefly presented. Then, in Section III analysis of the control approach through complex harmonic transfer functions is carried on. The accuracy of the control algorithms is assessed by simulation results, shown in Section IV, where the improvement on local voltage unbalance and total harmonic distortion is quantified by figures-of-merit. Section V points out design issues related to the switching frequency, and Section VI presents the main conclusions.

II. SYSTEM ARCHITECTURE AND CONTROL STRATEGY

A. System architecture

As can be seen in Fig. 1, only the local voltage at the PCC and the local converter output current are measured by the controller, characteristics which distinguish the proposed control strategy from conventional ones measuring the load current beyond the PCC for voltage support.

B. Stationary reference frames

The converter output line currents and the PCC line voltages are denoted by real vectors in the abc stationary frame as

$$\mathbf{i}_{abc} = \begin{bmatrix} i_a & i_b & i_c \end{bmatrix}^T$$
$$\mathbf{v}_{abc} = \begin{bmatrix} v_a & v_b & v_c \end{bmatrix}^T. \tag{1}$$
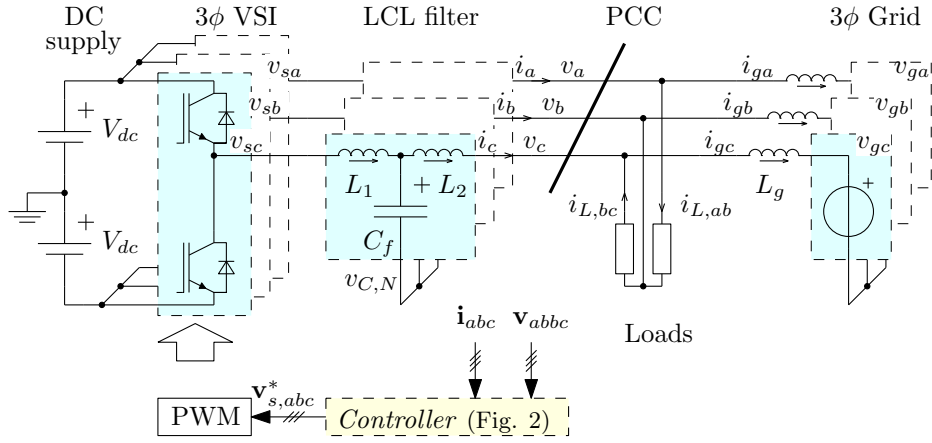
Fig. 1. Diagram of a grid-connected three-phase three-wire voltage-source converter system with local loads.

Because of practical convenience, stationary reference frames are applied in the rest of this paper for the control of three-phase GCC voltage and current quantities. The line currents and voltages in (1) are transformed to the $\alpha\beta$ quantities as

$$\mathbf{i}_{\alpha\beta} = \mathbf{T}_C \mathbf{i}_{abc}$$
$$\mathbf{v}_{\alpha\beta} = \mathbf{T}_C \mathbf{v}_{abc} \tag{2}$$

where $\mathbf{T}_C$ is a Clarke transformation matrix,

$$\mathbf{T}_C = \frac{2}{3} \begin{bmatrix} 1 & -1/2 & -1/2 \\ 0 & \sqrt{3}/2 & -\sqrt{3}/2 \end{bmatrix}. \tag{3}$$

In (2), the corresponding signals in the $\alpha\beta$ reference frame are denoted as

$$\mathbf{i}_{\alpha\beta} = \begin{bmatrix} i_\alpha & i_\beta \end{bmatrix}^T$$
$$\mathbf{v}_{\alpha\beta} = \begin{bmatrix} v_\alpha & v_\beta \end{bmatrix}^T. \tag{4}$$

Furthermore, in order to take advantage of the circuit symmetry in Fig. 1 , the real-valued $\alpha\beta$ quantities are grouped in complex numbers

$$\underline{i}_{\alpha\beta} = i_\alpha + j i_\beta$$
$$\underline{v}_{\alpha\beta} = v_\alpha + j v_\beta. \tag{5}$$

In the following, it should be noted that the symbols fo real vectors and matrices are in bold, symbols with a underline, e.g. $\underline{(.)}$, represent complex quantities or transfer function polynomials with complex coefficients, and, unless mentioned otherwise, symbols without a underline bar denote real-valued quantities or transfer functions with only real-valued polynomial coefficients.

C. Control strategy

This section elaborates on the structure of the controller in Fig. 1 for add-on voltage support. Note that the two objectives of the control strategy are to regulate the active power injection and to support the local voltage simultaneously. Since the average (not the instantaneous) active power is dominantly determined by the fundamental positive-sequence component of the converter output current, the active (and reactive) power injection can be controlled by regulating the fundamental positive-sequence component of the converter output current. At the same time, because the fundamental negative-sequence components and other harmonics hardly contribute to the average active power, they can be regulated to correct the local voltage for unbalanced and harmonic compensation. Therefore, the controller is composed of two loops: one for the control of the output current fundamental positive-sequence component and the other for the regulation of the PCC voltage fundamental negative-sequence component and other harmonics.

Accordingly, a parallel current-voltage control architecture is considered in this paper, because it can well generalize a current controller [2], [3], a hybrid current-voltage control scheme [5], [6] and a parallel scheme. Fig. 2 shows the block diagram of the current-voltage control architecture. The current reference consists of only fundamental positive-sequence component, whose magnitude is formulated by an active power regulation loop shown in Fig. 3.

The current and voltage controllers in Fig. 2 are decoupled in the frequency domain, following [11]:

$$\underline{C}_{i,\alpha\beta}(s) = K_p + K_i \frac{\omega_1}{s} + K_{res,1}^+ \underline{H}_{res,1}^+(s)$$
$$\underline{C}_{v,\alpha\beta}(s) = K_{res,1}^- \underline{H}_{res,1}^-(s) + K_{res,h} \sum_{h \in \mathbb{N}_h} H_{res,h}(s) \tag{6}$$

in which normalized complex transfer functions are given by

$$\underline{H}_{res,1}^+(s) = \frac{\omega_1}{s - j\omega_1 + \delta_1 \omega_1}$$
$$\underline{H}_{res,1}^-(s) = \left(\frac{\omega_1}{s + j\omega_1 + \delta_2 \omega_1} \right) \left(\frac{s - j\omega_1}{s - j\omega_1 + \delta_4 \omega_1} \right)$$
$$H_{res,h}(s) = \frac{\omega_1 s}{s^2 + \delta_3(2h\omega_1)s + (h\omega_1)^2} \tag{7}$$

where ω_1 is the fundamental angular grid frequency, and δ_1, δ_2, δ_3 and δ_4 are damping factors to shape the bandwidth of the resonant filters in order to improve convergence to steady-state operation [12]. Further, K_p, K_i, $K_{res,1}^+$, $K_{res,1}^-$ and $K_{res,h}$ in (6) are real-valued adjustable gains that should be designed for accuracy and stability.
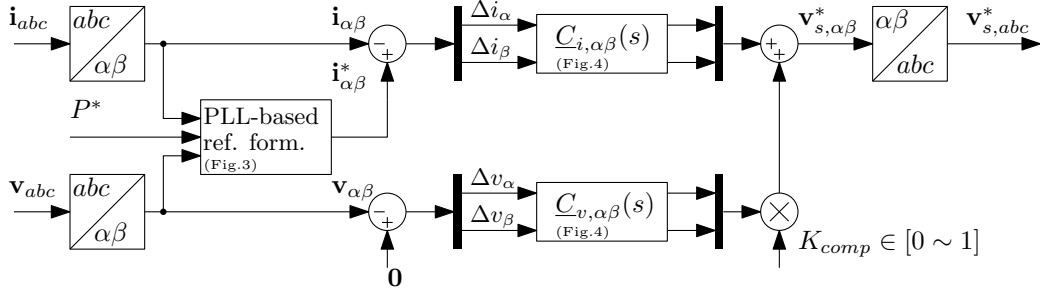
Fig. 2. Block diagram of decoupled (and, at last, integrated) current and voltage control in stationary reference frame.
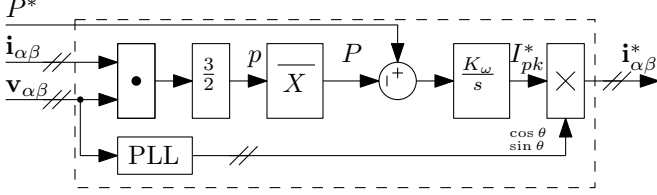

Fig. 3. Diagram of the control loop for (average) active power regulation.
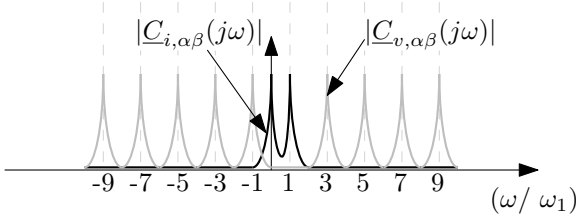

Fig. 4. Complementary operation of the current and voltage resonant controllers in Fig. 2, as function of frequency.

Fig. 4 illustrates the complementary operation of the resonant current and voltage controllers. As outlined, the current controller works actively at the zero and positive fundamental frequencies ($\{0, 1\}$), and, complementarily, the voltage controller works actively at the negative fundamental and harmonic frequencies ($\{-h, \cdots, -3, -1, 3, \cdots h\}$). Note in (6) that, in order not to interfere with the control of the fundamental positive-sequence component in the GCC system output current, the harmonic sequence component of order $h = 1$ is not included but attenuated by a notch filter in the voltage controller ($1 \notin N_h$).

III. MODELING AND ANALYSIS OF THE CLOSED-LOOP CONVERTER SYSTEM

In this section a frequency-domain equivalent model is derived for the closed-loop three-phase three-wire GCC system in Fig. 2.

A. Open-loop system modeling

Neglecting the PWM switching-frequency harmonics, the per-phase two-level VSI is modelled as a controlled average voltage source, as depicted in Fig. 5.

B. Equivalent sequence model

It is assumed that the devices of the 3ϕ LCL filters in Fig. 5 (inverter-side inductor Z_1, filter capacitor Z_c and grid-side inductor Z_2) are identical for each phase, and the mid-point voltage of the LCL filter, $v_{C,N}$, is referenced to the middle point of the dc supply. Therefore, the relation between per-phase currents and voltages can be described as

$$\frac{\mathbf{v}^*_{s,abc}}{Z_1(s)} - \frac{\mathbf{v}_{abc}}{Z_1(s)} - \frac{Z_2(s)}{Z_1(s)}\mathbf{i}_{abc} =$$

$$= \mathbf{i}_{abc} + \frac{\mathbf{v}_{abc}}{Z_c(s)} + \mathbf{i}_{abc}\frac{Z_2(s)}{Z_1(s)} - \frac{1}{Z_c(s)}\begin{bmatrix} v_{C,N}(s) \\ v_{C,N}(s) \\ v_{C,N}(s) \end{bmatrix}. \quad (8)$$

Applying the Clarke transformations of (2) to (8) results in

$$\frac{\mathbf{v}^*_{s,\alpha\beta}}{Z_1(s)} - \frac{\mathbf{v}_{\alpha\beta}}{Z_1(s)} - \frac{Z_2(s)}{Z_1(s)}\mathbf{i}_{\alpha\beta} = \mathbf{i}_{\alpha\beta} + \frac{\mathbf{v}_{\alpha\beta}}{Z_c(s)} + \mathbf{i}_{\alpha\beta}\frac{Z_2(s)}{Z_c(s)}. \quad (9)$$

After some rearrangements, (9) becomes

$$\mathbf{i}_{\alpha\beta} = -\frac{1}{Z_o(s)}\mathbf{v}_{\alpha\beta} + \frac{k(s)}{Z_o(s)}\mathbf{v}^*_{s,\alpha\beta} \quad (10)$$

in which

$$k(s) = \frac{Z_c(s)}{Z_c(s) + Z_1(s)} \quad (11)$$

$$Z_o(s) = \frac{Z_c(s)Z_1(s)}{Z_c(s) + Z_1(s)} + Z_2(s) \quad (12)$$

where the gain $k(s)$ and the equivalent open-loop impedance $Z_o(s)$ are determined from the LCL filter parameters, being
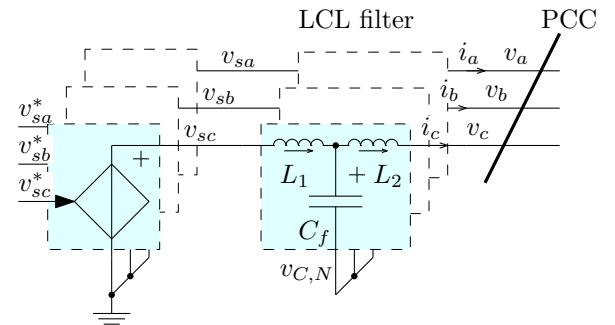

Fig. 5. Circuit representation of the 3-phase 3-wire GCC system in Fig. 1 in open loop control.
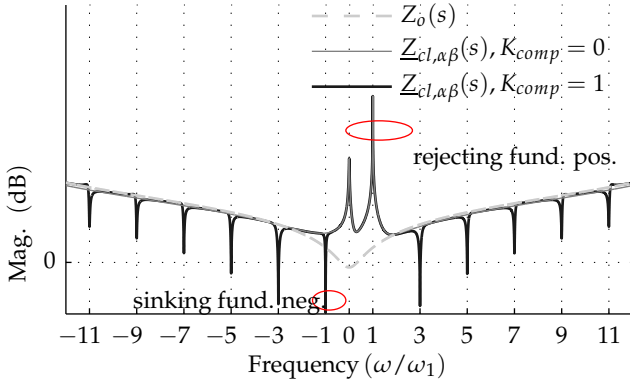
Fig. 6.   Magnitude of the closed-loop GCC system equivalent output impedance as function of frequency, in comparison to the converter natural impedance.

therefore designated hereafter as the converter natural gain and impedance, respectively.

In view of the symmetric and decoupled impedances, the definitions in (5) are applied to (10), yielding a reduced open-loop model description in complex quantities as

$$\underline{i}_{\alpha\beta}(s) = \frac{k(s)}{Z_o(s)} \underline{v}^*_{s,\alpha\beta}(s) - \frac{1}{Z_o(s)} \underline{v}_{\alpha\beta}(s) \qquad (13)$$

which is a much more convenient representation for control design purposes of the three-phase GCC system.

C. Closed-loop system sequence model

In view of (13), the control law in Fig. 2 is rewritten as

$$\underline{v}^*_{s,\alpha\beta}(s) = (\underline{i}^*_{\alpha\beta}(s) - \underline{i}_{\alpha\beta}(s))\underline{C}_{i,\alpha\beta}(s) - K_{comp}\underline{v}_{\alpha\beta}(s)\underline{C}_{v,\alpha\beta}(s) \qquad (14)$$

where $\underline{i}^*_{\alpha\beta}(s)$ is the current reference. Combining the controller in (14) and the plant model in (10) yields

$$\underline{i}_{\alpha\beta}(s) = \underline{i}^*_{\alpha\beta}(s)\underline{k}_{cl,\alpha\beta}(s) - \frac{1}{\underline{Z}_{cl,\alpha\beta}(s)}\underline{v}_{\alpha\beta}(s) \qquad (15)$$

where $\underline{k}_{cl,\alpha\beta}(s)$ corresponds to an equivalent gain of a controllable current source with equivalent internal impedance $\underline{Z}_{cl,\alpha\beta}(s)$. It is found from (14) that

$$\underline{k}_{cl,\alpha\beta}(s) = \frac{\underline{C}_{i,\alpha\beta}(s)k(s)}{Z_o(s) + \underline{C}_{i,\alpha\beta}(s)k(s)}$$

$$\underline{Z}_{cl,\alpha\beta}(s) = \frac{Z_o(s) + \underline{C}_{i,\alpha\beta}(s)k(s)}{1 + K_{comp}\underline{C}_{v,\alpha\beta}(s)k(s)} \qquad (16)$$

where $K_{comp} \in [0 \sim 1]$ is a so-called compensating effort index. When $K_{comp} = 0$, no active voltage support is provided since only the current controller loop is active.

D. Closed-loop output impedance

Fig. 6 shows the magnitude of the complex output impedance $\underline{Z}_{cl,\alpha\beta}(s)$ in (16) as function of frequency.

The equivalent impedance is enhanced for the harmonic sequence components of order $\{0, 1\}$ and, compared to the converter natural impedance, lowered for the components of order $\{-11, \cdots, -3, -1, 3, \cdots 11\}$. As already illustrated [12], the grouped $\alpha\beta$-signal of order $h = 1$ corresponds

TABLE I
PARAMETERS OF THE THREE-PHASE THREE-WIRE GCC SYSTEM IN FIG. 1

Description	Symbol	Value
Supply voltage	V_{dc}	400V
PWM frequency	f_{sw}	10kHz
VSI-side inductor	L_1	3.6mH (0.4Ω)
Filtering capacitor	C_f	10μF (0.4Ω)
Grid-side inductor	L_2	2.0mH (0.4Ω)
Grid impedance	L_g	6mH(0.2Ω)
Grid per phase voltage	$V_{g,rms}$	220V
Grid frequency	f_g	50Hz

TABLE II
CONTROLLER PARAMETERS IN REFERENCE TO (6)

Component	Quantity	Value	Quantity	Value
Controller $\underline{C}_i(s)$	K_p	10	K_i	0.32
	$K^+_{res,1}$	4.78	δ_1	$2 \cdot 10^{-3}$
Controller $\underline{C}_v(s)$	$K^-_{res,1}$	0.25	δ_2	$4 \cdot 10^{-3}$
	$K_{res,h}$	0.20	$\mathbb{N}_h$	$\{3,5, \ldots 11\}$
	δ_3	10^{-3}	δ_4	0.10
Power loop	K_ω	$\omega_1/4000$	ω_1	$2\pi f_g$

to the fundamental positive-sequence components, $h = 0$ to the dc component, and $h = -1$ to the fundamental negative-sequence components. Therefore, under the proposed control strategy the sensitivity of the output current of the closed-loop converter to the fundamental positive-sequence and dc disturbance from the PCC voltage is lowered, and it is enhanced with respect to the fundamental negative-sequence and harmonic disturbances .

IV. SIMULATION RESULTS

The parameters of the three-phase three-wire GCC system (in reference to Fig. 1) in Table I are used for simulation tests. The controller parameters are listed in Table II.

A. Double-side harmonic spectrum

For the purpose of analysis of positive- and negative-sequence harmonic components, the double-side harmonic spectrum of the PCC voltage is represented as a complex Fourier series

$$\underline{v}_{\alpha\beta}(t) = \sum_{h \in \mathbb{Z}} V_h e^{jh\omega_1 t} e^{j\varphi_h} \qquad (17)$$

where $\mathbb{Z}$ is a set of integer numbers, and V_h and φ_h are the respective magnitude and initial phase of the synthesized harmonic sequence component of order h. As such, V_h denotes a positive- or negative-sequence harmonic component amplitudes when $h > 0$ and $h < 0$, respectively. Otherwise stated, the double-side harmonic spectrum in (17) allows for a compact representation of both harmonic and unbalance distortion of three-phase quantities, and it is applied to assess the local voltage quality in the sequence.

In order to quantify the quality of three-phase current/voltage signals like in (17), a figure-of-merit, so-called total harmonic distortion, is defined as

$$\text{THD}_{ps} = \frac{\sqrt{\sum_{h\in\mathbb{Z}, h\neq 1} V_h^2}}{V_1^2} \qquad (18)$$

which is calculated in relation to the fundamental positive-sequence component of the signal.

B. Local voltage support

As mentioned earlier, the GCC output impedance for the harmonic and unbalanced components can be adjusted (by changing K_{comp}) for different degrees of local voltage support.

1) $K_{comp} = 0$: When the voltage support controller is disabled, the output impedance of the GCC system for the harmonic and unbalanced components is determined by the LCL filter. The simulation results in this case are shown in Fig. 7.

2) $K_{comp} = 0.1$: Fig. 8 shows the results when K_{comp} is set deliberately small in order to shape the output impedance of the GCC system to an intermediate low value (see Fig. 6 and (16)). It can be seen from Fig. 8 that compared to the results in Fig. 7, the total harmonic distortion of the PCC voltage and the grid current is reduced.

3) $K_{comp} = 1$: In Fig. 9 the compensation index is set to unity. In this case, the equivalent GCC output impedance for the targeting harmonic sequence signals of order $\{-11, \cdots, -3, -1, , 3, \cdots, 11\}$ is forced lower. It can be seen that, compared to the case in Fig. 8, the total harmonic distortion of the PCC voltage and the grid current is significantly reduced.

Summarizing, it can be seen from Figs.7 to 9 that increasing the compensation index K_{comp} helps to reduce the distortion of the local PCC voltage and grid current, which is in agreement with analysis of the harmonic transfer functions in Fig. 6. When K_{comp} is zero, the LCL filter is dominant in determining the GCC system output impedance for grid unbalanced and harmonic components. This makes the GCC control insensitive to unbalanced and harmonic disturbances from the grid. An increased K_{comp} enhances the control sensitivity, allowing the GCC system to compensate for a desired level of the local unbalanced or non-linear load currents.

C. Current reference step for active power regulation

Steering of active power flow is illustrated in Fig. 10. The current reference for active power regulation (I_{pk}^* in Fig. 3) steps from 0A to 6A. As a result, it is shown that, while also performing local voltage support as in Fig. 9, the GCC system achieves fast and stable tracking of the desired current components related to active power flow control.

V. IMPACT OF THE SWITCHING FREQUENCY

Due to its good performance regarding tracking of sinusoidal references, a first-order resonant filter at the grid fundamental frequency is selected for positive-sequence current control in (6), which sets the needed phase shift with respect
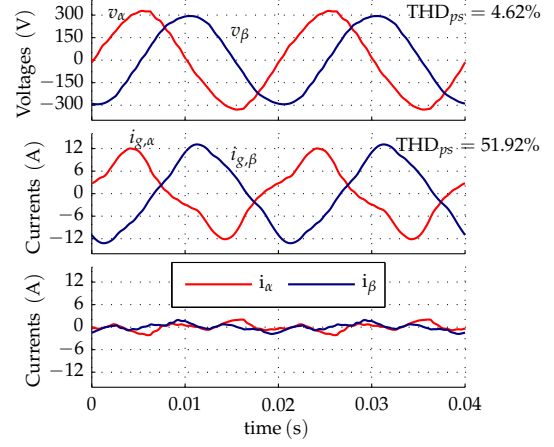

Fig. 7. Simulation results showing that the voltage harmonic distortion is slightly reduced when the GCC is operational and $K_{comp} = 0$.
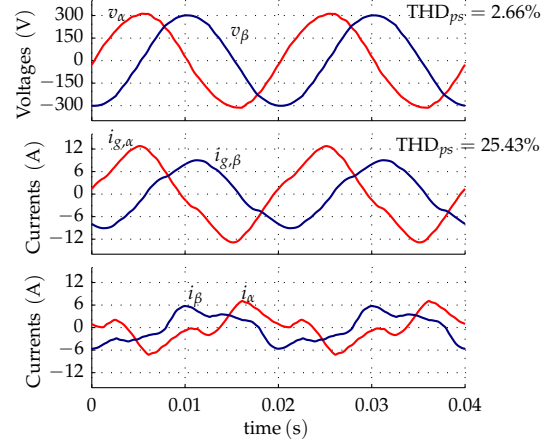

Fig. 8. Simulation results showing that the voltage harmonic distortion is further reduced when the GCC is operational and $K_{comp} = 0.1$.
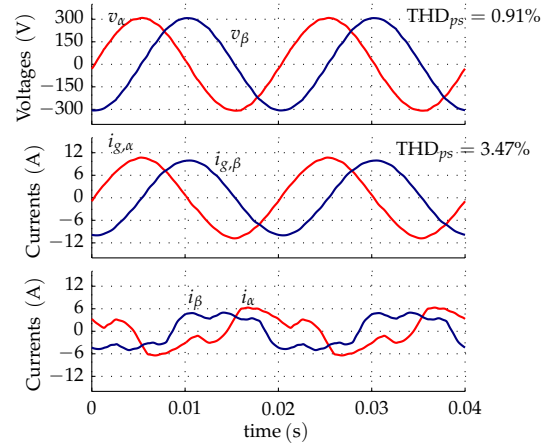

Fig. 9. Simulation results showing that the voltage harmonic distortion is significantly reduced when the GCC is operational and $K_{comp} = 1$.

to the fundamental grid voltage component (yielding therefore the desired charge/discharge active and reactive power flow). Voltage support is also achieved through first- and second-order resonant filters in (6) to attenuate a selection of harmonic components other than the fundamental one.
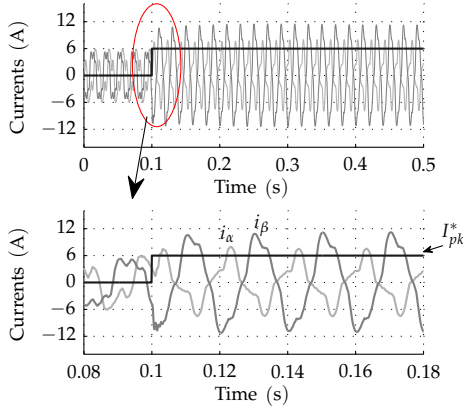
Fig. 10. Simulation results showing the GCC system's response when the current reference steps up aiming at an increase of active power transfer. The initial conditions (only voltage support before 0.1s) are the same as in Fig.9.

It is a common practical design recommendation to choose in (6) no more than a maximal number of harmonics to be attenuated such that $h < |h|_{\max}$, with

$$|h|_{\max} = 0.1 \, \omega_s/\omega_1$$

where ω_s is the angular switching frequency and ω_1 the fundamental angular grid frequency. Furthermore, with regard to control stability and accuracy, the values of the adjustable gains for the first- and second-order filters in (6) should be high enough but limited, preferably chosen such that

$$K_{res,1}^+ = \omega_c L_2 \ \text{with} \ \omega_c \leq 0.1 \, \omega_s$$
$$K_{res,1}^-, K_{res,h} \ll \omega_c/\omega_1.$$

Therefore, the higher the switching frequency ω_s, the broader the design choices for achieving good filter performance. Due to superior material properties, wide band-gap semiconductors enable higher voltages, switching frequencies, and operating temperatures when compared to conventional Si technology. As a consequence, SiC semiconductors lead to the advancement of the proposed filtering methods aiming at improving power quality in distribution grids.

VI. Conclusion

The proposed control scheme for three-phase three-wire grid-connected converters consists of two decoupled loops, one for current control and another for voltage support. The local voltage at the PCC is measured and used in both loops: in one loop the voltage fundamental component is extracted via a PLL for converter output current synchronization with the grid; and in the other path the full voltage profile is used for unbalance and harmonic compensation. The resulting duty-cycle value that steers the pulse-width modulation of the converter switching legs is just the sum of the two previously calculated duty-cycles by each control loop. Since no external sensors beyond the PCC are required, the approach is readily applicable to already existing GCC systems as add-on local voltage support.

Results from numerical simulations validate the performance of the method, showing grid current harmonic distortion being reduced from 51.92% to 3.47% and PCC voltage distortion from 4.62% to 0.91%. The superior material properties of the next SiC generation allows an advanced practical realization of the proposed algorithms.

REFERENCES

[1] H. Fujita and H. Akagi, "The unified power quality conditioner: the integration of series and shunt-active filters," *IEEE Transactions on Power Electronics*, vol. 13, no. 2, pp. 315–322, Mar. 1998.

[2] B. Singh and C. Jain, "A decoupled adaptive noise detection based control approach for a grid supportive SPV system," *IEEE Transactions on Industry Applications*, vol. 53, no. 5, pp. 4894–4902, Sep. 2017.

[3] R. S. R. Chilipi, N. A. Sayari, K. H. A. Hosani, and A. R. Beig, "Adaptive notch filter-based multipurpose control scheme for grid-interfaced three-phase four-wire DG inverter," *IEEE Transactions on Industry Applications*, vol. 53, no. 4, pp. 4015–4027, Jul. 2017.

[4] Z. Dai, H. Lin, H. Yin, and Y. Qiu, "A novel method for voltage support control under unbalanced grid faults and grid harmonic voltage disturbances," *IET Power Electronics*, vol. 8, no. 8, pp. 1377–1385, 2015.

[5] F. Nejabatkhah, Y. W. Li, and B. Wu, "Control strategies of three-phase distributed generation inverters for grid unbalanced voltage compensation," *IEEE Transactions on Power Electronics*, vol. 31, no. 7, pp. 5228–5241, Jul. 2016.

[6] C. Xu, K. Dai, X. Chen, and Y. Kang, "Unbalanced PCC voltage regulation with positive- and negative-sequence compensation tactics for MMC-DSTATCOM," *IET Power Electronics*, vol. 9, no. 15, pp. 2846–2858, 2016.

[7] F. H. M. Rafi, M. J. Hossain, and J. Lu, "Improved neutral current compensation with a four-leg PV smart VSI in a LV residential network," *IEEE Transactions on Power Delivery*, vol. 32, no. 5, pp. 2291–2302, Oct. 2017.

[8] S. D'Arco, M. Ochoa-Gimenez, L. Piegari, and P. Tricoli, "Harmonics and interharmonics compensation with active front-end converters based only on local voltage measurements," *IEEE Transactions on Industrial Electronics*, vol. 64, no. 1, pp. 796–805, Jan. 2017.

[9] X. Zhao, L. Meng, C. Xie, J. M. Guerrero, X. Wu, J. C. Vasquez, and M. Savaghebi, "A voltage feedback based harmonic compensation strategy for current-controlled converters," *IEEE Transactions on Industry Applications*, vol. PP, no. 99, pp. 1–1, 2017.

[10] M. M. Shabestary and Y. A. I. Mohamed, "Advanced voltage support and active power flow control in grid-connected converters under unbalanced conditions," *IEEE Transactions on Power Electronics*, vol. 33, no. 2, pp. 1855–1864, Feb. 2018.

[11] Y. Zhang, M. G. L. Roes, M. A. M. Hendrix, and J. L. Duarte, "Symmetric-component decoupled control of grid-connected inverters for voltage unbalance correction and harmonic compensation," *International Journal of Electrical Power & Energy Systems*, vol. 115, p. 105490, Feb. 2020.

[12] F. Wang, M. C. Benhabib, J. L. Duarte, and M. A. M. Hendrix, "Sequence-decoupled resonant controller for three-phase grid-connected inverters," in *Twenty-Fourth Annual IEEE Applied Power Electronics Conference and Exposition*, Feb. 2009, pp. 121–127.